Effects of surfactant on lift coefficients of bubbles in linear shear flows

Hayashi, Kosuke

Tomiyama, Akio

(Citation)
International Journal of Multiphase Flow,99:86-93

(Issue Date)
2018-02

(Resource Type)
journal article

(Version)
Accepted Manuscript

Effects of Surfactant on Lift Coefficients of Bubbles in Linear Shear Flows

Kosuke Hayashi[1*], Akio Tomiyama[1]

hayashi@mech.kobe-u.ac.jp, tomiyama@mech.kobe-u.ac.jp

[1]Graduate School of Engineering, Kobe University, 1-1 Rokkodai, Nada, Kobe 657-8501, Japan

*Corresponding author: Tel & Fax: +81-78-803-6108, hayashi@mech.kobe-u.ac.jp

Abstract

Effects of surfactant on the lateral motion of bubbles in linear shear flows are numerically investigated by using an interface tracking method. Ranges of the bubble Reynolds number Re, Eötvös number Eo, Morton number M and dimensionless shear rate Sr are $2 < Re < 70$, $0.6 < Eo < 5$, $10^{-6} < M < 10^{-4}$ and $0 \leq Sr < 1$, respectively. The main conclusions obtained are as follows: (1) the lift coefficient, C_L, of a bubble decreases as the Langmuir number increases, (2) the surfactant decreases the critical values of Eo and Re, at which C_L changes its sign, (3) the reduction in C_L of bubbles of large Hatta numbers due to the presence of surfactant can be understood from the surface tension reduction, and (4) the Marangoni force affects C_L of small Hatta number bubbles, and therefore, the surface immobilization effect of the Marangoni force should be taken into account to model C_L of contaminated bubbles.

Keywords: Contaminated bubble, Marangoni effect, Interface tracking simulation

Highlights

Effects of surfactant on lift coefficient are investigated.

Lift coefficient can be correlated by accounting for reduction in surface tension.

Validation for clean bubbles is conducted using experimental data.

1. Introduction

Knowledge on lift force acting on a bubble is of great importance to understand the mechanism of the gas phase distributions of bubbly flows in various gas-liquid two-phase systems. The lift force, $\boldsymbol{F}_L$, acting on a bubble is often modeled as (Zun, 1980; Auton, 1987)

$$\boldsymbol{F}_L = -C_L \rho_L \frac{\pi d^3}{6} (\boldsymbol{V}_B - \boldsymbol{V}_L) \times \nabla \times \boldsymbol{V}_L \tag{1}$$

where C_L is the lift coefficient, ρ_L the liquid density, d the sphere-volume equivalent bubble diameter, $\boldsymbol{V}_B$ the bubble velocity, and $\boldsymbol{V}_L$ the liquid velocity. Auton (1987) derived C_L of a spherical bubble in a linear shear flow at a high bubble Reynolds number. For spherical bubbles at low Reynolds numbers, Legendre and Magnaudet (1997) derived an analytical solution of C_L, which is a function of the bubble Reynolds number and the dimensionless shear rate. In addition, they carried out numerical simulations of spherical bubbles in linear shear flows by using a boundary-fitted coordinate (BFC) method and proposed a semi-empirical correlation of C_L applicable to spherical bubbles for a wide range of the Reynolds number (Legendre and Magnaudet,

1998). These studies showed that C_L of a spherical bubble is positive at any Reynolds numbers.

Negative C_L have been observed for deformed bubbles. Tomiyama et al. (1993) carried out two-dimensional volume-tracking simulations of bubbles flowing in linear shear flows. The C_L of a deformed bubble becomes negative with increasing the Eötvös number. The reversal of the sign of C_L was also confirmed in BFC (Takagi et al., 1995) and front-tracking simulations (Ervin and Tryggvason, 1997). Tomiyama et al. (2002) carried out experiments on the lift force acting on bubbles in linear shear flows and proved that C_L decreases with increasing the Reynolds number or the Eötvös number and changes its sign at certain values of these dimensionless groups. They also proposed an empirical correlation of C_L, which is a function of the Reynolds number for low bubble Reynolds numbers and that of a modified Eötvös number for relatively higher Reynolds numbers. The lift forces acting on deformed bubbles and drops at low Reynolds numbers are theoretically studied by Magnaudet et al. (2003). They derived analytical solutions for the inertia-induced and the deformation-induced lift forces. The deformation-induced lift force explains the reversal of lift force acting on the deformed bubbles in the above-mentioned experiments and simulations (Adoua et al., 2009). Adoua et al. (2009) numerically investigated the lift force acting on ellipsoidal bubbles at intermediate and high Reynolds numbers and described that the cause of the negative lift force is the interaction between the vorticity of the linear shear flow and that generated at the bubble surface. Though the above-mentioned studies revealed the underlying physics in the reversal of the sign of C_L of clean bubbles and some C_L correlations have been proposed (Tomiyama et al., 2002; Dijkhuizen et al, 2010), our knowledge on the lift force acting on contaminated bubbles is still insufficient.

Takagi et al. (2009) pointed out that a surface-active agent (surfactant) drastically changes the flow structure of an upward bubbly flow consisting of bubbles of 0.8-1.0 mm ID, that is, bubbles in the presence of surfactant at a low surfactant concentration are apt to migrate toward the channel wall and consequently bubble clusters are formed near the wall, whereas fully contaminated bubbles do not migrate toward the wall and no bubble clusters are formed. They also carried out BFC simulations of 1.0 mm single spherical bubbles contaminated with surfactant using a stagnant-cap model and successfully explained the surfactant effect on cluster formation. Fukuta et al. (2008) also conducted BFC simulations for contaminated spherical bubbles of 0.5 mm and confirmed that C_L for bubbles of low degree of contamination mainly consists of the pressure component and its sign is positive, whereas the increase in the degree of contamination makes the pressure contribution smaller and C_L becomes negative due to the viscous stress at the interface. These studies focused only on the surfactant effect on the lift force acting on spherical bubbles, and that on deformed bubbles has been rarely investigated.

Numerical simulations of spherical and deformed bubbles in linear shear flows of contaminated liquids are carried out in this study to investigate the effects of surfactant on the lift force. An interface tracking method proposed in our previous study (Hayashi and Tomiyama, 2012; 2014) is used for this purpose.

2. Field equations and numerical methods

The continuity and momentum equations for incompressible Newtonian fluids based on one-fluid formulation are given by

$$\nabla \cdot \boldsymbol{V} = 0 \tag{2}$$

$$\frac{\partial \boldsymbol{V}}{\partial t} + \boldsymbol{V} \cdot \nabla \boldsymbol{V} = -\frac{1}{\rho}\nabla P + \frac{1}{\rho}\nabla \cdot \mu[\nabla \boldsymbol{V} + (\nabla \boldsymbol{V})^T] + \boldsymbol{g} + \frac{1}{\rho}[\sigma\kappa \boldsymbol{n} + \nabla\sigma]\delta \tag{3}$$

where $\boldsymbol{V}$ is the velocity, t the time, P the pressure, $\boldsymbol{g}$ the acceleration of gravity, ρ the density, μ the viscosity, σ the surface tension, κ the mean curvature, $\boldsymbol{n}$ the unit normal to the interface, δ the delta function, which is non-zero only at the interface, and the superscript T denotes the transpose. The term, $(\nabla\sigma)\delta$, is the tangential component of surface tension force, i.e. the Marangoni force. The level set function, ϕ, (Sussman et al., 1994) is used to track the interface, i.e.

$$\frac{\partial \phi}{\partial t} + \boldsymbol{V} \cdot \nabla \phi = 0 \tag{4}$$

The interface is represented by the so-called zero level set, $\phi = 0$. The fluid properties in the vicinity of the interface are smoothed as

$$\rho = (1 - H_\varepsilon)\rho_G + H_\varepsilon \rho_L \tag{5}$$

$$\mu = (1 - H_\varepsilon)\mu_G + H_\varepsilon \mu_L \tag{6}$$

where the subscripts G and L denote the gas and liquid phases, respectively, and H_ε is the smoothed Heaviside function defined by (Sussman et al., 1994)

$$H_\varepsilon = \begin{cases} 0 & \text{if } \phi \le -\varepsilon \\ \dfrac{1}{2}\left[1 + \dfrac{\phi}{\varepsilon} + \dfrac{1}{\pi}\sin\left(\dfrac{\pi\phi}{\varepsilon}\right)\right] & \text{if } |\phi| < \varepsilon \\ 1 & \text{if } \phi \ge \varepsilon \end{cases} \tag{7}$$

where 2ε is the thickness of the smoothed interface region. The re-initialization equation for the level set function is solved at each time step to recover the property of the level set function as the distance function. The $\boldsymbol{n}$ and κ are evaluated as $\boldsymbol{n} = \nabla\phi/|\nabla\phi|$ and $\kappa = -\nabla\cdot\boldsymbol{n}$, respectively. A global volume correction method (Meier, 2000) is utilized to conserve fluid volumes. The ghost fluid method (Kang et al., 2000) is adopted to evaluate the normal component of the surface tension force. The continuum surface force model (Brackbill et al., 1992) is utilized to evaluate the Marangoni force (Hayashi and Tomiyama, 2012; 2014).

The transport equation of surfactant in the liquid phase and that at the interface are given by (Levich, 1962; Stone, 1990; Cuenot et al., 1997)

$$\frac{\partial C}{\partial t} + \boldsymbol{V}\cdot\nabla C = \nabla\cdot D_C \nabla C \tag{8}$$

$$\frac{\partial \Gamma}{\partial t} + \nabla_S\cdot\Gamma\boldsymbol{V} = \nabla_S\cdot D_S\nabla_S\Gamma + \dot{S}_\Gamma \tag{9}$$

where C is the surfactant concentration in the liquid phase, Γ the surfactant concentration at the interface, and D_C and D_S are the diffusion coefficient in the liquid phase and that at the interface, respectively. The source term $\dot{s}_\Gamma$ is the molar flux from the liquid phase to the interface due to the adsorption and desorption and is evaluated

by using the Frumkin-Levich model (Frumkin and Levich, 1947; Levich, 1962; Cuenot et al., 1997):

$$\dot{S}_\Gamma = k[C_S(\Gamma_{max} - \Gamma) - \beta\Gamma] \tag{10}$$

where k and β are the parameters for the adsorption and desorption kinetics, respectively, Γ_{max} the saturation value of Γ, and C_S the molar concentration in the liquid phase in the vicinity of the interface.

The surface tension is calculated using (Rosen and Kunjapp, 2012)

$$\sigma(\Gamma) = \sigma_0\left[1 + \frac{R_G T \Gamma_{max}}{\sigma_0}\ln\left(1 - \frac{\Gamma}{\Gamma_{max}}\right)\right] \tag{11}$$

where σ_0 is the surface tension of a clean interface, R_G the universal gas constant, and T the temperature.

Equation (8) is solved using the method proposed by Muradoglu and Tryggvason (2008), in which the interfacial molar flux of surfactant is added to the equation as the volumetric source term. The Γ is extrapolated into both phases to facilitate the computation of the surface gradient in Eq. (9) (Xu and Zhao, 2003).

See Hayashi and Tomiyama (2012; 2014) for the detail of the method and its validation for clean and contaminated bubbles in stagnant liquids.

3. Numerical condition

The computational domain is shown in Fig. 1. The domain size is 16d x 16d x 16d in the x, y and z directions, respectively. In the present calculations, the bubble is assumed to move in the x-z plane and the flow is symmetric with respect to the x-z plane crossing the bubble center. Therefore only a half of the flow domain (16d, 8d, 16d) is computed as shown in the figure. The experimental data obtained in our previous study (Aoyama et al., 2017) confirm that flows are symmetric under the present numerical conditions. A linear shear flow with the velocity gradient ω enters from the top boundary at z = 16d. The continuous outflow condition is imposed on the bottom boundary, i.e. the velocity gradient in the z-direction is zero at z = 0, whereas the pressure is constant. Moving walls are used for the boundaries at x = 0 and 16d. The boundary conditions at y = 0 and 8d are continuous outflow and symmetric, respectively. The change in the domain size from 14d to 18d caused a little difference in predicted lift coefficients.

Bubbles are initially spherical and are placed in the domain center. Uniform computational cells, whose widths are d/28, are used near the bubble (inside the box represented by dotted lines in the figure), whereas non-uniform coarser cells are used for the other region. The cell size in the latter region gradually increases in the manner of the geometric sequence, where the equal ratio is determined based on the number of cells (Nakahashi and Fujii, 1995). Grid convergence tests were carried out and the results showed that C_L of clean and contaminated bubbles were converged with this spatial resolution. The rise velocities, W, of the single bubbles are estimated using the experimental database (Aoyama et al., 2017) and the velocities of the moving walls at y = 0 and 16d are determined so as to set the inlet velocity at x = 8d at $-W$. Owing to this

setup, the bubbles were kept inside the uniform fine cell region throughout the simulations.

The Morton number defined by

$$M = \frac{\mu_L^4 \Delta\rho g}{\rho_L^2 \sigma^3} \tag{12}$$

are log$M$ = −3.9 and −5.5. Here $\Delta\rho = \rho_L - \rho_G$. These values of M are the same as those used in our experimental study (Aoyama et al., 2017). The fluid properties are given in Table 1. The velocity gradients ω are 3.2 and 7.4 s^{-1}. The surfactant properties will be described in Sec. 4.2.

The drag and lift coefficients were evaluated by substituting predicted bubble velocity and its acceleration into the equation of motion of a bubble. See Aoyama et al. (2017) for more detail of the evaluation method.

4. Results and discussion

4.1 Validation of the method

Comparisons between measured (Aoyama et al., 2017) and predicted bubble shapes at log$M$ = −5.5 and ω = 3.2 s^{-1} are shown in Figs. 2(a) and (b) (solid lines), where Eo, Re and Sr are the Eötvös number, the bubble Reynolds number and the dimensionless shear rate defined by

$$Eo = \frac{\Delta\rho g d^2}{\sigma_0} \tag{13}$$

$$Re = \frac{\rho_L |\boldsymbol{V}_R| d}{\mu_L} \tag{14}$$

$$Sr = \frac{\omega d}{|\boldsymbol{V}_R|} \tag{15}$$

where $\boldsymbol{V}_R$ (= $\boldsymbol{V}_B - \boldsymbol{V}_L$) is the relative velocity. The shape flattens with increasing *Eo* and *Re*. The dimensionless shear rates are much smaller than unity. At these small values of *Sr*, the bubbles are not so much slanted due to the shear flow and the shapes are almost axisymmetric. As shown in Fig. 3(b), the increase in ω gradually deteriorates the axisymmetry of the deformed bubble. In all the cases, the predicted shapes agree well with the experiments.

Figure 4 shows a comparison of measured and predicted bubble aspect ratios *E*. The aspect ratio is defined as the ratio of the bubble minor axis to the major axis. The influence of the shear rate on *E* is small both in the prediction and the experimental data. The dependence of *E* on *d* is predicted well.

The drag coefficients C_D are shown in Fig. 5. For bubbles at ω = 0 s^{-1}, the predictions agree with the experiments and C_D calculated using correlations of C_D and *E* proposed by Rastello et al. (2011) and the authors (Aoyama et al., 2015), respectively. The increase in ω increases C_D at large *Re* in the experimental data. On the other hand, in the numerical simulations, C_D is independent of ω. Further investigations should be carried out in the future to clarify the *Sr* effect on C_D.

Lift coefficients are plotted against *Re* in Fig. 6. The bubble of *d* = 1 mm are almost spherical at both log*M* (Fig. 4) and their *Re* are small (*Re* < 1). The experimental

data of their C_L agree with the Legendre-Magnaudet correlation for spherical bubbles (1998) given by

$$C_L = \sqrt{\left(\frac{6}{\pi^2} \frac{2.255}{\sqrt{SrRe}[1+0.2Sr/Re]^{3/2}} \right)^2 + \left(\frac{1}{2} \frac{Re+16}{Re+29} \right)^2} \tag{16}$$

At higher Reynolds numbers, C_L gradually decreases as Re increases. The Legendre-Magnaudet correlation is no longer applicable to the deformed bubbles. For this range of Re, the effect of Sr on C_L is small. The increase in Re makes C_L negative. The predictions agree well with the experimental data.

Tomiyama et al. (2002) pointed out that C_L of deformed bubbles at intermediate Re and Eo are well correlated in terms of the modified Eötvös number defined by

$$Eo_H = \frac{\Delta\rho g d_H^2}{\sigma_0} \tag{17}$$

where d_H is the major axis of a bubble. Figure 7 shows the C_L plotted against Eo_H. Although C_L slightly depends on M, Eo_H is useful in correlating C_L in the present range of the dimensionless groups. The predicted C_L shows a fair agreement with the experimental data. It should however be noted that, for a wider range of M, C_L of deformed bubbles are not well correlated only with Eo_H and the viscous effect should be taken into account (Aoyama et al., 2017).

4.2 Surfactant effect on C_L

4.2.1 Large Hatta number cases

Surfactant properties are k = 5.08 m^3/mol·s, β = 21.7 mol/m^3, Γ_{max} = 5.9x10^{-6} mol/m^2, D_C = 1.1x10^{-9} m^2/s and D_S = 1.1x10^{-9} m^2/s. These values are for 1-pentanol in the air-water system (Takagi et al., 2009). The initial bulk concentrations, C_∞, are 30 and 300 mol/m^3. The Langmuir number, which is the ratio of the adsorption rate to the desorption rate

$$La = \frac{C_\infty}{\beta}, \tag{18}$$

at C_∞ = 30 and 300 mol/m^3 are 1.38 and 13.8, respectively. Hence the adsorption and desorption fluxes are comparable with each other in the former, whereas the adsorption flux is much larger than the desorption flux in the latter.

Figure 8 shows shapes and velocity fields of clean and contaminated bubbles at log$M$ = −5.5, Eo = 3.49 and ω = 3.2 s^{-1}, where Γ* = Γ/Γ_{max}, σ* = σ/σ_0 and Ha is the Hatta number defined by

$$Ha = \frac{kC_\infty d}{|\boldsymbol{V}_R|} \tag{19}$$

The surfactant makes the bubble shape more flattened. The Γ* increases from the nose to the rear. The large Ha means that the adsorption is much faster than the bubble rising speed, in other words the speed of advection at the interface. The Γ* is therefore high over the whole surface. Especially, Γ* in the rear region is close to the saturation value of Γ. Due to the high concentration, the reduction of surface tension is remarkable, that

is, σ* ranges from 0.33 to 0.55. The whole bubble surface is contaminated, but is still mobile, implying that the Marangoni effect is not strong. Figure 9 shows bubble shapes at a lower *Eo* and lower *Re*. The ω is 3.2 s^{-1} and 7.4 s^{-1} in Fig. 9(a) and (b), respectively. The increase in ω breaks the left-right symmetry of the bubble shape as in the clean bubble case. The range of σ^* is more or less the same in these cases.

The drag coefficients of contaminated bubbles are plotted against the bubble Reynolds number in Fig. 10. The increase in *La* increases C_D and C_D at the highest *La* are close to those of solid particles (Schiller and Naumann, 1933)

$$C_D = \frac{24}{Re}(1 + 0.15Re^{0.678}) \tag{20}$$

The shear rate does not have much influence on C_D both for clean and contaminated bubbles.

Figure 11 shows C_L of the contaminated bubbles. The increase in *La* decreases C_L at both Morton numbers, and therefore, the critical *Re* decreases. On the C_L-Eo_H plane, C_L of the deformed bubbles at different *La*, of course, differ from each other due to the C_L reduction as shown in Fig. 12.

It is known that the terminal velocity of a clean Taylor bubble at low Morton numbers can be correlated in terms of the Eötvös number only (White and Beardmore, 1962). The authors (Hayashi and Tomiyama, 2012) simulated contaminated Taylor bubbles rising through vertical pipes using the same numerical method. The numerical results showed that the terminal velocity of a low Morton number Taylor bubble contaminated with surfactant depends on the surface tension near the bubble nose and

can be evaluated by making use of available correlations for clean Taylor bubbles, provided that the degree of contamination near the bubble nose is known and the Marangoni effect in the nose region is negligible. As discussed above, C_L of the clean bubbles can be correlated in terms of Eo_H in the present M range and the Marangoni effect on the contaminated bubbles is not large. Hence it is expected that C_L of the deformed bubbles in contaminated liquids can be correlated in terms of Eo_H using the surface tension reduced by surfactant, i.e.,

$$Eo_H(\sigma_{eq}) = \frac{\Delta\rho g d_H^2}{\sigma_{eq}} \tag{21}$$

where σ_{eq} (= $\sigma(\Gamma_{eq})$) is the surface tension in the adsorption-desorption equilibrium ($\dot{s}_\Gamma = 0$) in the absence of fluid flows and the concentration, Γ_{eq}, in the equilibrium is given by $\Gamma_{eq} = La\Gamma_{max}/(1 + La)$. In Fig. 13, C_L of the contaminated bubbles are re-plotted against $Eo_H(\sigma_{eq})$. Good agreement between C_L of the clean and contaminated bubbles implies that the surfactant effect on C_L of bubbles contaminated with the present surfactant is due to the surface tension reduction.

4.2.2 Small Hatta number cases

Simulations of contaminated bubbles are carried out with the surfactant properties of k = 50 m^3/mol·s, β = 6.6x10^{-4} mol/m^3, Γ_{max} = 2.9x10^{-6} mol/m^2, D_C = 3.0x10^{-10} m^2/s and D_S = 3.0x10^{-10} m^2/s, which are for Triton X-100 in the air-water system (Takagi et al., 2009). The C_∞ is 0.16 mol/m^3, which gives a large Langmuir number, i.e. La = 240. Hence the adsorption is much dominant in the adsorption-desorption kinetics.

Figure 14(a) shows a shape and a velocity field of a contaminated bubble, whose *Ha* is much smaller than the simulations in the previous section. The surfactant adsorbing in the nose region immediately flows toward the rear and accumulates in the rear region due to the small *Ha*, which results in a large surface tension gradient in the bubble side region. Consequently the bubble surface is partly immobile, that is, the upper surface is nearly free-slip and the internal circulation is formed, whereas the surface velocity is close to zero and the internal circulation is attenuated in the lower part of the bubble. In addition, the Marangoni force mitigates shape deformation. The surface immobilization effect is clearer for a smaller bubble as shown in Fig. 14(b), i.e. the internal circulation almost vanishes.

The C_L of small *Ha* bubbles are shown in Fig. 15. Lift coefficients of spherical solid particles predicted using BFC (Kurose and Komori, 1999) are also shown in the figure. The C_L of solid particles approaches to zero as *Re* increases. Although the bubble surface is apt to be immobile, C_L of bubbles can take negative values. This may be attributed to the shape deformation. Figure 16 shows C_L plotted against $Eo_H(\sigma_{eq})$. The C_L cannot be correlated only with $Eo_H(\sigma_{eq})$ since the Marangoni effect is significant in these cases. This effect, therefore, should be taken into account when modeling C_L of contaminated bubbles of small *Ha*.

5. Conclusion

Interface tracking simulations of clean and contaminated bubbles in linear shear flows were carried out to investigate effects of surfactant on the lateral motion of bubbles. The numerical method was based on a level set method, and the adsorption-desorption kinetics was taken into account. Ranges of *Eo*, *Re*, *M* and *Sr*

were $2 < Re < 70$, $0.6 < Eo < 5$, $10^{-6} < M < 10^{-4}$ and $0 \leq Sr < 1$, respectively. Two kinds of surfactants were used to examine contaminated bubbles of large and small Hatta numbers. The conclusions obtained are as follows:

1. The lift coefficient, C_L, of a bubble decreases as the Langmuir number increases.

2. The surfactant decreases the critical values of Eo and Re, at which C_L changes its sign, due to the C_L reduction.

3. The C_L of deformed bubbles at large Hatta numbers can be correlated in terms of the modified Eötvös number with the reduced surface tension, in other words, the reduction in C_L due to the presence of surfactant can be understood from the surface tension reduction if the Marangoni force is not significant.

4. The Marangoni force has non-negligible influence on C_L when the Hatta number is small, and therefore, the surface immobilization effect of the Marangoni force should be taken into account to model C_L of contaminated bubbles.

Acknowledgement

The authors would like to thank Mr. Shohei Aoyama and Mr. Takeshi Hamada for their assistance. This work has been supported by JSPS KAKENHI 15H03920 and 17K06158.

References

Adoua, R., Legendre, D., Magnaudet, J., Reversal of the lift force on an oblate bubble in a weakly viscous linear shear flow, *Journal of Fluid Mechanics* 628, 23-41, 2009.

Aoyama, S., Hayashi, K., Hosokawa, S., Lucas, D., Tomiyama, A., Lift force acting on single bubbles in linear shear flow, *International Journal of Multiphase Flow*, 96, 113-122, 2017.

Aoyama, S., Hayashi, K., Hosokawa, S., Tomiyama, A., Shapes of ellipsoidal bubbles in infinite stagnant liquids, *International Journal of Multiphase Flow* 79, 23–30, 2016.

Auton, T., The lift force on a spherical body in a rotational flow, *Journal of Fluid Mechanics* 183, 199-218, 1987.

Brackbill, J. U., Kothe, D. B., Zemach, C., A continuum method for modeling surface tension, *Journal of Computational Physics* 100, 335-354, 1992.

Cuenot, B., Magnaudet, J., Spennato, B., The effects of slightly soluble surfactants on the flow around a spherical bubble, *Journal of Fluid Mechanics* 339, 25-53, 1997.

Ervin, E. A., Tryggvason, G., The rise of bubbles in a vertical shear flow, *Journal of Fluids Engineering* 119, 443-449, 1997.

Frumkin, A., Levich, V. G., On surfactants and interfacial motion, *Zhurnal Fizicheskoi Khimii* 21, 1183–1204, 1947, in Russian.

Fukuta, M., Takagi, S., Matsumoto, Y., Numerical study on the shear-induced lift force acting on a spherical bubble in aqueous surfactant solutions, *Physics of Fluids* 20(4), 040704, 2008.

Hayashi, K., Tomiyama, A., Effects of surfactant on terminal velocity of a Taylor bubble in a vertical pipe, *International Journal of Multiphase Flow* 39, 78-87, 2012.

Kang, M., Fedkiw, R. P., Liu, X.-D., A boundary condition capturing method for multiphase incompressible flow, *Journal of Scientific Computing* 15, 323-360, 2000.

Kurose, R. and Komori, S., Drag and lift forces on a rotating sphere in a linear shear flow, *Journal of Fluid Mechanics*, 384, 183-206, 1999.

Legendre, D., Magnaudet, J., A note on the lift force on a spherical bubble or drop in a low-Reynolds- number shear flow, *Physics of Fluids*, 9, 3572-3574, 1997.

Legendre, D., Magnaudet, J., The lift force on a spherical bubble in a viscous linear shear flow, *Journal of Fluid Mechanics* 368, 81-126, 1998.

Levich, V. G., *Physicochemical hydrodynamics*, Prentice Hall, 1962.

Magnaudet, J., Takagi, S., Legendre, D., Drag, deformation and lateral migration of a buoyant drop moving near a wall, *Journal of Fluid Mechanics* 476, 115-157, 2003.

Meier, M., Towards a DNS of multiphase flow, *Laboratorium fur Kerntechnik Institutfu fur Energietechnik*, Technical Report No. LKT–01–00, ETH Zurich, 2000.

Muradoglu, M., Tryggvason, G., A front-tracking method for computation of interfacial flows with soluble surfactants, *Journal of Computational Physics* 227, 2238-2262, 2008.

Nakahashi, K., Fujii, K., Grid Generation and Computer Graphics, University of Tokyo Press, Tokyo, Japan, 1995.

Rastello, M., Marié, J.-L., Lance, M., 2011. Drag and lift forces on clean spherical and ellipsoidal bubbles in a solid-body rotating flow. *Journal of Fluid Mechanics* 682, 434–459, 2011.

Rosen, M. J. and Kunjappu, J. T., Surfactants and Interfacial Phenomena, Wiley, 2012.

Stone, H. A., A simple derivation of the time-dependent convective-diffusion equation for surfactant transport along a deforming interface, *Physics of Fluids A* 2, 111-112, 1990.

Schiller, L., Naumann, A. Z., Uber die grundlegende Berechunung bei der Schwekraft-aufbereitung, *Zeitschrift des Vereines Deutscher Ingenieure* 44, 318-320, 1933.

Sussman, M., Smereka, P., Osher, S., A level set approach for computing solutions to incompressible two-phase flow, *Journal of Computational Physics* 114, 146-159, 1994.

Takagi, S., Matsumoto, Y., Three dimensional calculation of a rising bubble, *Proc. of the 2nd International Conference on Multiphase Flow*, PD2, 9-16, 1995.

Takagi, S., Ogasawara, T., Fukuta, M., Matsumoto, Y., Surfactant effect on the bubble motions and bubbly flow structures in a vertical channel, *Fluid Dynamics Research* 41(6), 065003, 2009.

Tomiyama, A., Zun, I., Sou, A., Sakaguchi, T., Numerical analysis of bubble motion with the VOF method, *Nuclear Engineering and Design* 141, 69-82, 1993.

Tomiyama, A., Tamai, H., Zun, I., Hosokawa, S., Transverse migration of single bubbles in simple shear flows, *Chemical Engineering Science* 57, 1849-1858, 2002.

White, E.T., Beardmore, R.H., The velocity of rise of single cylindrical air bubbles through liquids contained in vertical tubes, *Chemical Engineering Science* 17, 351-361, 1962.

Xu, J.-J., Zhao, H.-K., An Eulerian formulation for solving partial differential equations along moving interface, *Journal of Scientific Computing* 19, 573-594, 2003.

Zun, I., Transverse migration of bubbles influenced by walls in vertical bubbly flow, *International Journal of Multiphase Flow* 6, 583-588, 1980.

List of Figures

List of Tables

Table 1 Fluid properties

log$M$	−3.9	−5.5
ρ_L [kg/m^3]	1205	1180
μ_L [mPa·s]	47	18
σ [mN/m]	66	67
ρ_G [kg/m^3]	1.2	1.2
μ_G [Pa·s]	1.8x10^{-5}	1.8x10^{-5}

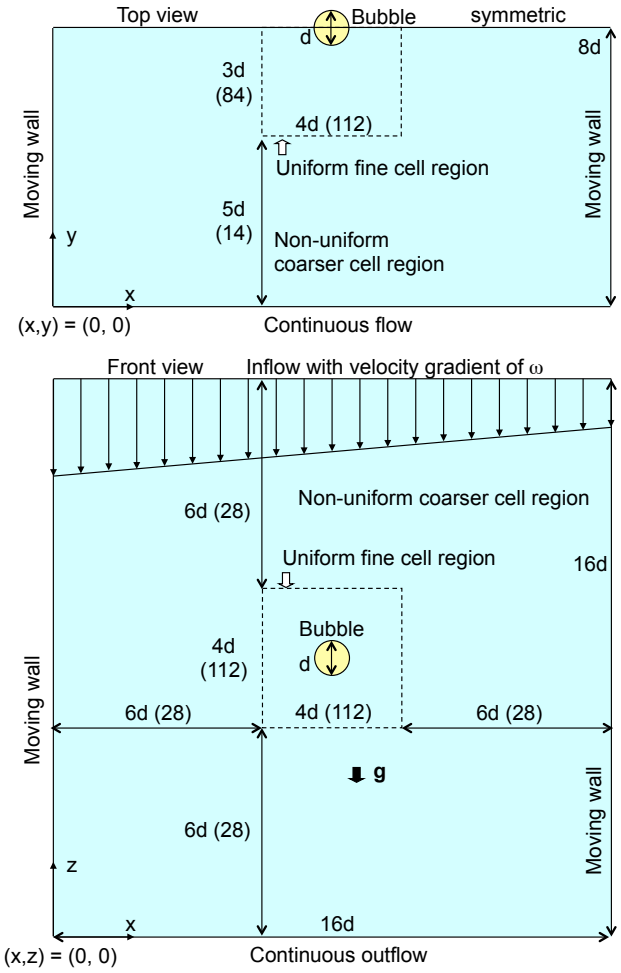

Fig. 1 Computational domain (values in parentheses are numbers of computational cells)

(a) $(Eo, Re, Sr) = (0.64, 15, 0.054)$ (b) $(2.8, 62, 0.056)$

Fig. 2 Comparisons of clean bubble shapes (solid lines) and experiment (photos) at $\log M = -5.5$ and $\omega = 3.2\ \mathrm{s}^{-1}$

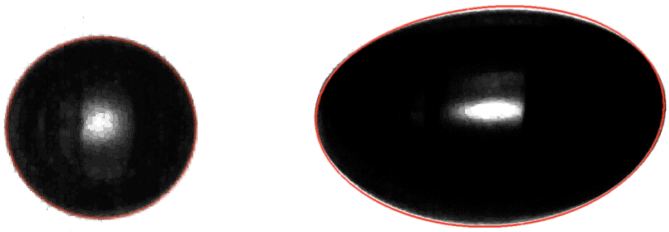

(a) (Eo, Re, Sr) = (0.65, 14, 0.13) (b) (2.8, 56, 0.14)

Fig. 3 Comparisons of clean bubble shapes in simulation (solid lines) and experiment (photos) at $\log M = -5.5$ and $\omega = 7.4\ s^{-1}$

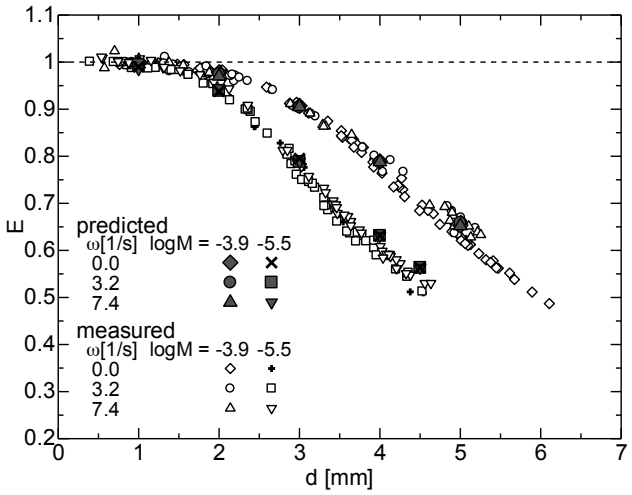

Fig. 4 Aspect ratios of clean bubbles in stagnant liquids and linear shear flows

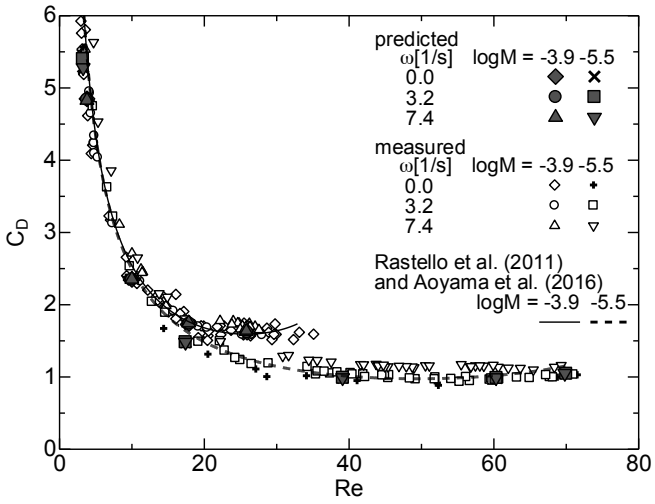

Fig. 5 Drag coefficients of clean bubbles in stagnant liquids and linear shear flows

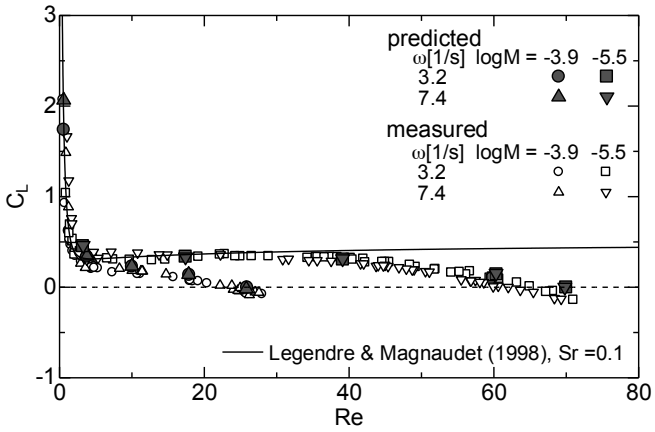

Fig. 6 Lift coefficients of clean bubbles

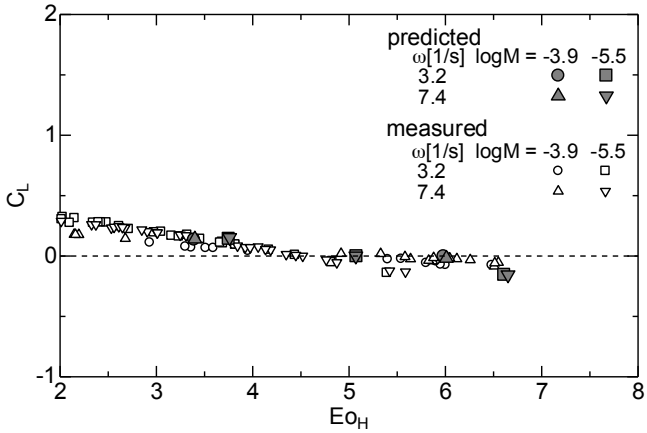

Fig. 7 Lift coefficients correlated in terms of Eo_H

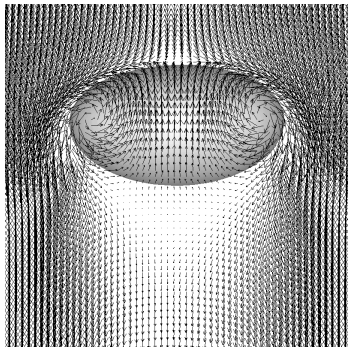

(a) clean (Re = 70, Sr = 0.061)

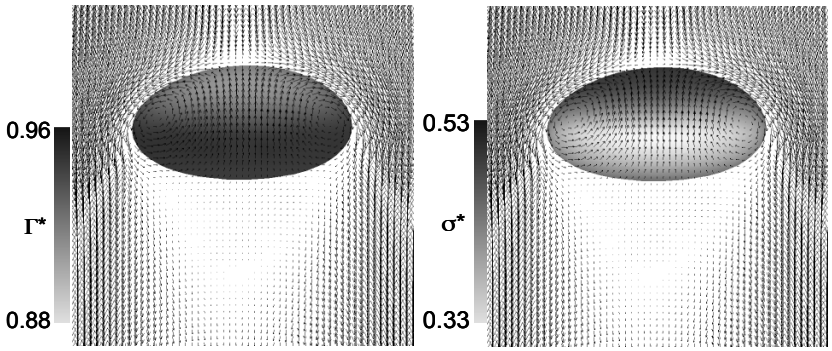

(b) contaminated (Re = 50, La = 13.8, Ha = 41, Ma = 4.8, Sr = 0.086, left: Γ^*, right: σ^*)

Fig. 8 Comparison of shape between clean and contaminated bubbles at log$M$ = −5.5, Eo = 3.49 and ω = 3.2 s^{-1}.

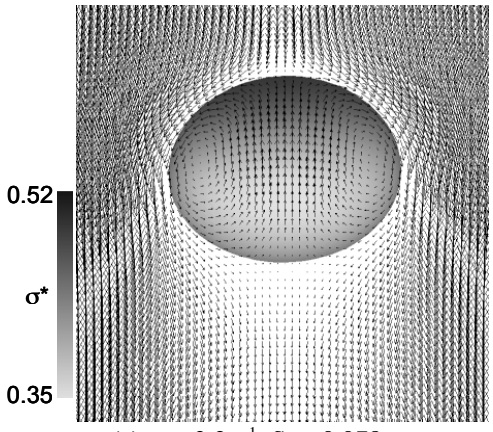

(a) ω = 3.2 s^{-1}, Sr = 0.078

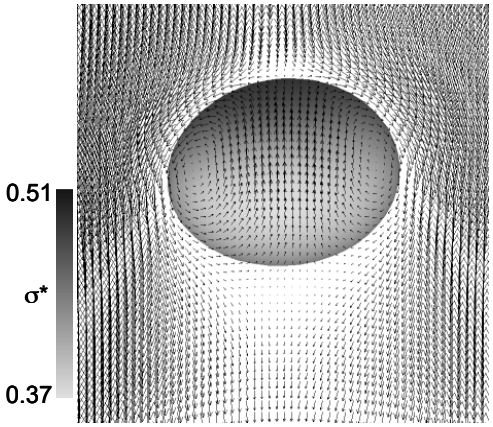

(b) ω = 7.4 s^{-1}, Sr = 0.18

Fig. 9 Effect of shear rate on contaminated bubble shape (log$M$ = −5.5, Eo = 1.55, Re = 24, La = 13.8, Ha = 37)

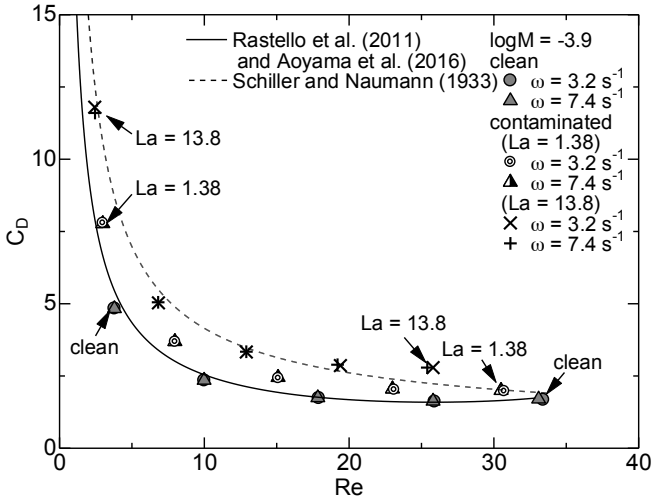

(a) log$M$ = –3.9

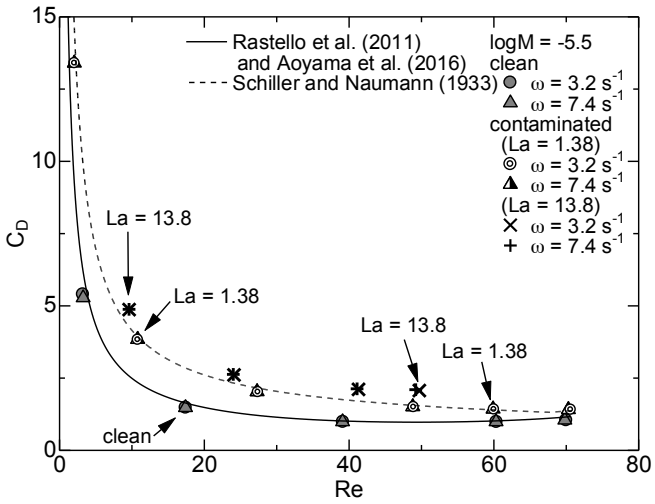

(b) log$M$ = –5.5

Fig. 10 Drag coefficients of bubbles contaminated with surfactant

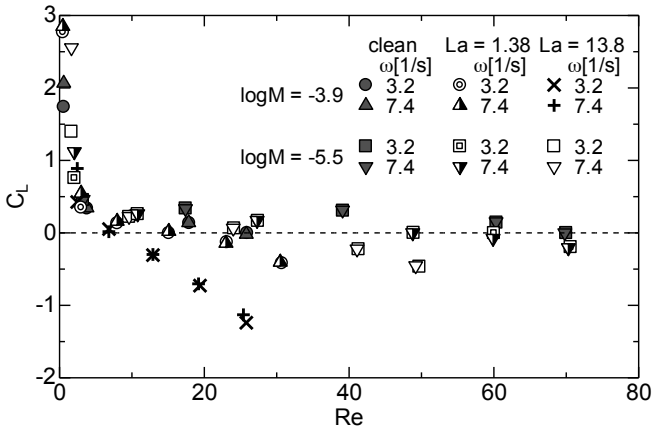

Fig. 11 Lift coefficients of bubbles contaminated with surfactant

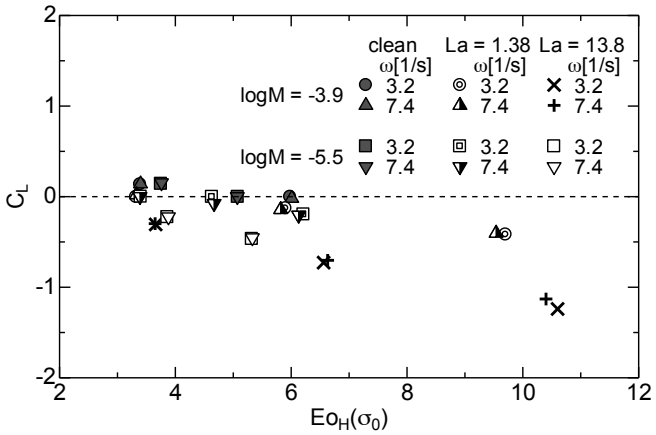

Fig. 12 Lift coefficients plotted against $Eo_H(\sigma_0)$

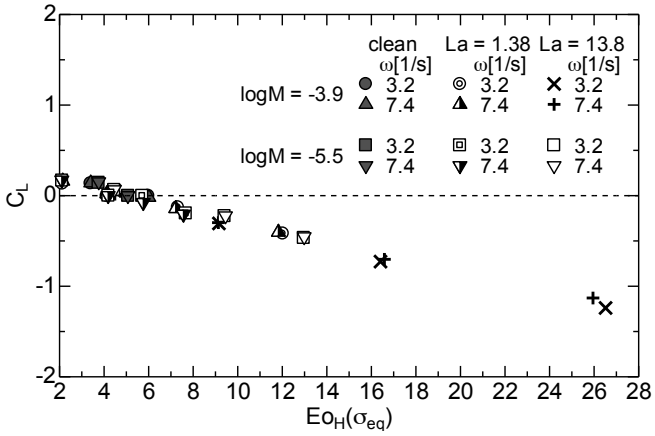

Fig. 13 Lift coefficients plotted against $Eo_H(\sigma_{eq})$

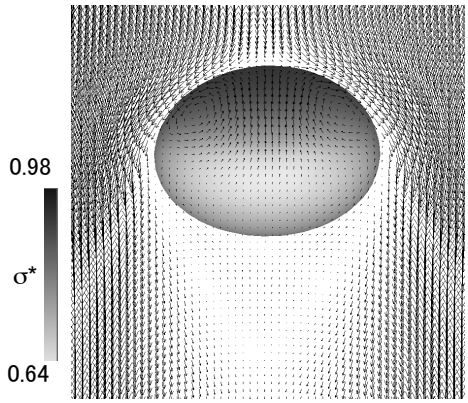

(a) log$M$ = –5.5, Eo = 3.49, ω = 3.2 s^{-1}, Re = 48.6, Ha = 0.213

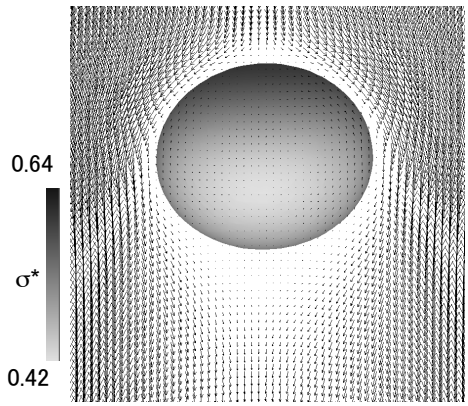

(b) log$M$ = –5.5, Eo = 1.55, ω = 3.2 s^{-1}, Re = 20.6, Ha = 0.224

Fig. 14 Contaminated bubbles of small Hatta numbers

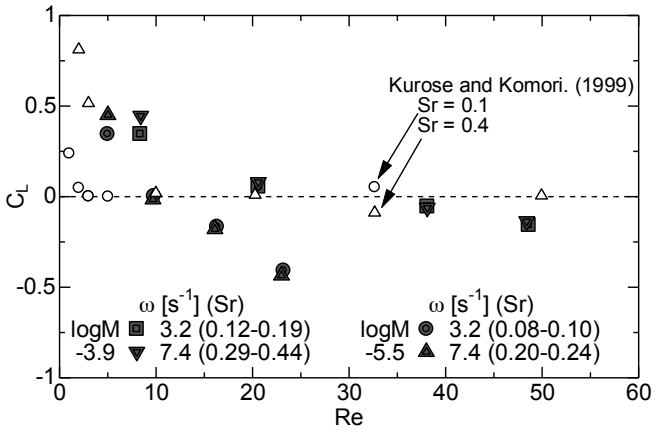

Fig. 15 Lift coefficients of bubbles of small Hatta numbers

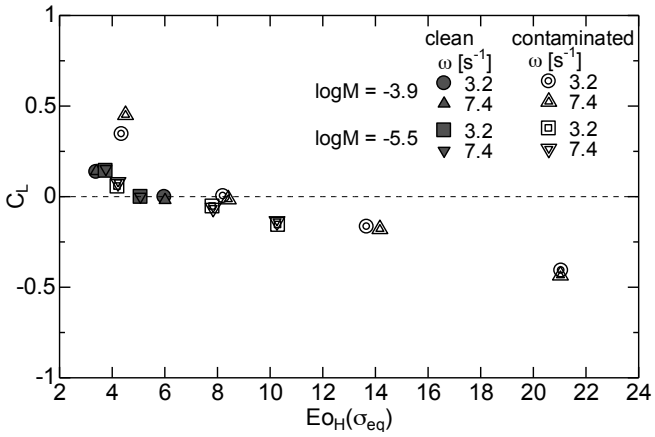

Fig. 16 Lift coefficients at small Hatta numbers plotted against $Eo_H(\sigma_{eq})$